Fundamental microwave-power-limiting mechanism of epitaxial high-temperature superconducting thin-film devices

P. Lahl[a] and R. Wördenweber
Institute of Thin Films and Interfaces (ISG) and Center of Nanoelectronic Systems for Information Technology (CNI), Forschungszentrum Jülich, Jülich 52425, Germany

(Received 8 November 2004; accepted 20 April 2005; published online 14 June 2005)

In this paper we present an experimental investigation of the nonlinear microwave properties of coplanar resonators patterned from epitaxial $Y_1Ba_2Cu_3O_{7-\delta}$ thin films in zero-field-cooled, field-cooled, and field-sweep experiments in the search for the fundamental limiting mechanism. The impact of magnetization, vortices, intrinsic limitation, grain boundaries, and thermal effects is evaluated. We find that the fundamental limiting mechanism in the absence of thermal and grain-boundary effects is given by the dc critical current density of the superconducting material which masks the intrinsic limitation expected at larger rf current densities. Demagnetizing effects, penetration barriers, vortex penetration, pinning, and relaxation of inhomogeneous vortex distributions are experimentally observed and in agreement with theoretical expectations. The experimental results are modeled in terms of a simple model for the power-handling capability which is based on a superposition of all current densities in the resonator and gives a consistent explanation of all experiments in magnetic fields and in zero field. © *2005 American Institute of Physics*. [DOI: 10.1063/1.1929088]

I. INTRODUCTION

The application of superconductors in microwave devices of large power densities (e.g., thin-film microwave devices) is limited by the onset of nonlinear effects which defines the power-handling capability of the devices. Naturally, intrinsic and extrinsic properties of superconductors convey limiting mechanisms compared to normal conducting materials. Thus, it is crucial to investigate and understand the *fundamental* microwave-power-limiting mechanisms of superconductors. Although considerable efforts are ongoing worldwide to uncover the fundamental nonlinear mechanisms responsible for the observed nonlinear effects, it is not completely understood.

The most important nonlinear effects are (i) the microwave-power-dependent losses, e.g., a nonlinear observed surface resistance

$$R_s(j) = R_0 + R_2^* j^2 + \cdots , \qquad (1)$$

(ii) the generation of harmonics, and (iii) the intermodulation distortions (IMD). Depending on the specific device, one of these effects might receive the most attention. However, it is clear from this simple phenomenology that as soon as one nonlinearity is present, all these nonlinear effects will arise.[1–5]

Various physical origins are considered in the discussion of the fundamental mechanism that will ultimately define the power-handling capability when all extrinsic mechanisms have been eliminated. Part of this discussion is whether this mechanism is field driven or current driven. Field-driven mechanisms are usually explained by a deterioration of the microwave properties due to the penetration of vortices if the surface magnetic rf field exceeds a certain limiting value of the order or based on B_{c1}.[6,7] However, by comparing measurements on devices with different-magnetic field configurations, it is argued that a field-driven mechanism cannot consistently describe the onset of nonlinear effects for all field configurations.[8] Current-driven mechanisms are usually based on the onset of nonlinear effects if the rf transport current density exceeds a certain limiting value which is characteristic of the nonlinear mechanism. If several current-driven mechanisms exist, the mechanism with the lowest limiting value then naturally defines the onset of nonlinear effects and, thus, the power-handling capability. The limiting value for the rf current density and its dependencies on physical quantities, such as temperature and magnetic field, then allows the identification of the specific current-limiting mechanism. A strong support for the idea of a current-driven limitation comes from power-handling capability measurements of the same thin superconducting films performed in two separate devices of highly different field configurations which give similar results as functions of the rf current density.[8]

From a dc perspective, there are three main current-limiting mechanisms: (i) grain-boundary Josephson junction behavior, (ii) pair breaking, and (ii) vortex depinning and motion.

The effect of grain-boundary Josephson junctions on the power-handling capability has been exemplary investigated using bicrystal grain boundaries of different misorientation angles. It has been found that the microwave-power-handling capability of yttrium–barium–copper oxide (YBCO) films is reduced from the overall thin-film values for misorientation angles of $\theta > 5°$ (Ref. 9) in agreement with IMD[10] and dc[11] experiments. Since epitaxial thin films are rated to contain misorientation angles of $\theta < 1°$, these experiments are a

[a]Electronic mail: p.lahl@fz-juelich.de

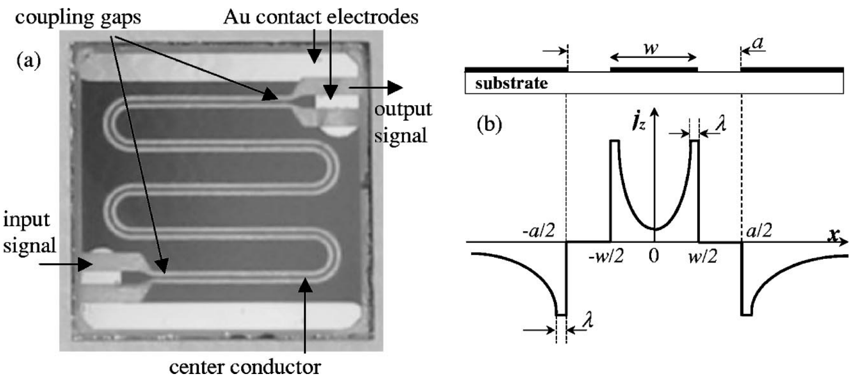

FIG. 1. (a) Top view of a superconducting thin-film coplanar resonator on a 12×12-mm substrate. (b) Cross section: schematic sketch of the design and microwave current distribution.

strong indication that the Josephson junction model does not represent the fundamental nonlinear mechanism for epitaxial high-T_c microwave devices.

Various investigations show that the limiting rf current density does not seem to agree with the pair-breaking mechanism since, on the one hand, the observed values are more than one order of magnitude below the pair-breaking critical current density $J_{c,\mathrm{PB}}$ and, on the other hand, they do not show the temperature dependence expected from models based on the pair-breaking mechanism.[12,13] It should be noted, however, that the pair-breaking mechanism seems to show extremely sensitive IMD measurements in the low-current limit due to a crossover with the vortex motion mechanism.[14]

Comparisons of the limiting rf current density with the dc critical current density associated to vortex motion have often been inconclusive so far (see, e.g., Ref. 12). On the one hand, such discussions are restricted to order-of-magnitude arguments since current densities are determined based on different criteria. On the other hand, it has to be explained how magnetic vortices can happen to appear in the superconductor. While this is clear in the case of field-cooled experiments, it has been argued that so called microwave vortices may be generated by the magnetic component of the rf field. We further point out that vortex–antivortex pairs may be generated by fluctuations and that these pairs may be broken up, e.g., thermally or by current densities, producing free vortices.

In this paper, we will present systematic investigations of the power-handling capability of YBCO coplanar resonators in magnetic fields, with the goal to investigate the impact of magnetic fields and vortices on the microwave properties and to identify the fundamental limiting mechanism for the onset of nonlinear microwave effects. The results suggest that (i) the limiting mechanism is current driven and (ii) that the dc critical current density represents the limitation for the rf power-handling capability in these experiments.

II. EXPERIMENTAL SETUP AND TECHNIQUE

All measurements presented in this paper were performed on coplanar thin-film $\lambda/2$ resonators (resonant frequency $f_0=1.4$ GHz) which were patterned photolithographically from epitaxial YBCO films (thickness $t\approx300$ nm). The YBCO films were deposited by magnetron sputtering on CeO_2-buffered r-cut sapphire substrates. For details on the sputter deposition process, please see Ref. 15 and references therein. The width of the resonator center conductor is $w=100\ \mu$m and the distance of the ground planes is $a=182\ \mu$m, yielding a transmission line impedance $Z_L=50\ \Omega$ [see Figs. 1(a) and 1(b).

One important aspect for the analysis of the rf power-handling capability is the rf current-density distribution in the device. For our geometry $(w>\lambda_L, t<\lambda_L)$, the theoretical description of the inhomogeneous electromagnetic-field distribution across the superconductor cross section is based on the solution of the integral equation of the rf magnetic-field distribution in the superconductor.[16–18] The resulting current distribution is obtained via a conformal mapping using the assumption of perfect conductivity and zero thickness of the coplanar line.[19,20] This solution contains an unphysical singularity at the edge of the superconductor. On the other hand, the magnetic screening current in the dc case at the surface is known from Pearl's model.[21] Combining this expression for the dc current distribution and the integral equation of the rf magnetic field at the edge of the superconductor, the solution for the rf current density at the edge of the superconductor of a coplanar resonator is given by[22]

$$J_z(x)=\frac{I_{\mathrm{rf}}}{wK\left(\frac{w}{a}\right)}\left\{\frac{\lambda_{\mathrm{eff}}}{w}\left[1-\left(\frac{w}{a}\right)^2\right]\right\}^{-1/2}$$

$$\text{for } \frac{w}{2}-\lambda_{\mathrm{eff}}\leqslant|x|\leqslant\frac{w}{2} \tag{2a}$$

and

$$J_z(x)=\frac{I_{\mathrm{rf}}}{wK\left(\frac{w}{a}\right)}\left\{\frac{\lambda_{\mathrm{eff}}}{a}\left[\left(\frac{a}{w}\right)^2-1\right]\right\}^{-1/2}$$

$$\text{for } \frac{a}{2}\leqslant|x|\leqslant\frac{a}{2}+\lambda_{\mathrm{eff}}, \tag{2b}$$

where I_{rf} is the total rf current, $K(w/a)$ is the complete elliptic integral which for our geometry is $K\approx1.72$, and λ_{eff} is the effective London penetration depth. The resulting current distribution is sketched in Fig. 1(b).

A number of aspects result from this current distribution which are important for our experiments: (i) The maximum current density in the ground plane is at least by a factor of $(w/a)^{1/2}$ smaller than in the center conductor. Therefore, the device properties are considered to be dominated by the center conductor. (ii) Due to the characteristic current distribution the power-handling capability is relatively small so that thermal effects can be neglected (see discussion below). (iii) Since the rf current is strongly peaked at the edge of the central conductor, these devices turn out to be highly sensitive to magnetization or vortex penetration. Therefore the microwave properties and the impact of vortices on the microwave properties can be investigated locally by establishing different vortex distributions in the resonator. Thus, the specific properties of coplanar microwave devices are ideal for the investigation of mechanisms that limit the power-handling capability.

The measurements were performed in a He flow cryostat and the measurement temperature could be adjusted in the range of 4.2 K to RT. An additional dc magnetic field of up to 0.6 T could be applied parallel to the *c* axis of the sample. The loaded quality factor of the resonator Q_L and the *S* parameters were measured in frequency domain using a network analyzer (HP8720D). The power-handling capability $P_{\max}$ is defined by the oscillating microwave power

$$P_{\rm osc} = Q_L P_{\rm in}, \tag{3}$$

at which the unloaded quality factor

$$Q_0 = Q_L(1 - S_{11} - S_{21})^{-1} \tag{4}$$

is degraded to 80% of its low-power value, i.e.,

$$Q_0(P_{\max}) = 0.8 Q_0(P \to 0), \tag{5}$$

with $Q_0 \approx 20.000\text{–}30.000$ for $P \to 0$ and $T \to 0$. In field-cooled (fc) and zero-field-cooled (zfc) experiments the resonator is cooled to the superconducting state in an applied magnetic field $B_{\rm fc}$ or in zero field, respectively. In field-cooled-sweep (fcs) experiments, the sample is first cooled to the superconducting state in an applied field $B_{\rm fc}$ (where the field-cooled state is established), and subsequently the field is modified by ΔB.

The measurements were carried out using a standard cryogenic system with computer control. Special measures were taken in order to optimize the measurement accuracy of *Q* and, thus, of $P_{\max}$ and reproducibility. We note that this was a prerequisite for presenting measurement curves of the power-handling capability in the detail shown below, especially in zero-field-cooled and field-cooled experiments.

III. RESULTS AND DISCUSSION

Figure 2 represents an overview of the dc magnetic-field dependence of the power-handling capability of a typical coplanar resonator in fc, zfc, and fcs experiments. The power handling capability $P_{\max}$ depends strongly upon the way the magnetic field is established. For fc experiments, a homogeneous vortex distribution is frozen in and the linear increase of the vortex density in the resonator results in a gradual decrease of the power-handling capability. In contrast, in the zfc case vortex penetration into the field-free superconductor occurs primarily in regions close to the surface of the superconductor, where the vortices are pinned. Thus, the maximum of this extremely inhomogeneous vortex distribution coincides with the maximum of the microwave current distribution at the edge of the central conductor, resulting in a strong reduction of $P_{\max}$ already at extremely small fields of a few microtesla. The following quite constant power-handling capability is consistent with other observations of flux penetration at small fields, where an increase of the magnetic field first leads only to a shift of the flux front into the superconductor.[23] Since the interior of the superconductor does not carry large rf currents, this shift does not affect the power-handling capability seriously. At larger magnetic fields, the fc and zfc values of $P_{\max}$ seem to merge. This is expected for the field, for which the zfc flux front approaches the center of the sample so that for the edge of the superconductor similar vortex densities for the fc and zfc cases can be expected.

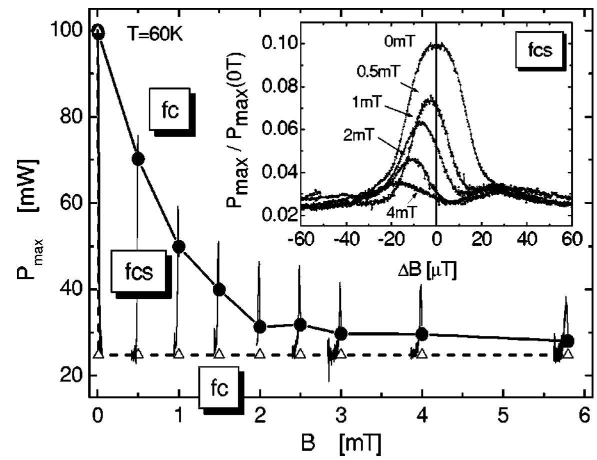

FIG. 2. Field dependence of the power-handling capability of a coplanar YBCO resonator for field-cooled (fc, solid circles), zero-field-cooled (zfc, open triangles), and field-cooled-sweep (fcs, solid lines) experiments. The inset shows the fcs measurement starting at different fields $B_{\rm fc}$ on a normalized scale as a function of field sweep ΔB.

In fcs experiments, the resulting field dependence of the power-handling capability represents a fingerprint of the processes of magnetization and vortex penetration (see inset of Fig. 2). This behavior can be understood by considering the effective magnetic field $B_{\rm eff}$ at the superconductor surface, which has contributions from the frozen-in magnetic field $B_{\rm fc}$ and the subsequent field change ΔB in the cold state

$$B_{\rm eff} = B_{\rm fc} + s\Delta B, \tag{6}$$

where,

$$s = (1 - D)^{-1} \tag{7}$$

is a dimensionless factor based on the demagnetizing factor *D* and $s \gg 1$ for our geometry. Since the frozen-in magnetic field does not cause a magnetization, the factor *s* has to be applied to the field change ΔB only. The effective surface magnetic field $B_{\rm eff}$ decays on the scale of the penetration depth λ into the superconductor. Since this coincides with the peaks of the rf current density at the superconductor surface, it is clear that the effective surface magnetic field $B_{\rm eff}$ and/or screening currents associated with it strongly affect the power-handling capability.

For small field changes ($|\Delta B| < 20\ \mu$T) the superconductor is magnetized as demonstrated by reversible field-cycling experiments (see Fig. 4). For $\Delta B > 0$ the effective magnetic field at the superconductor surface $B_{\rm eff}$ is increased, and, therefore, a decrease of the power-handling capability is observed. For $\Delta B < 0$ the frozen-in magnetic field B_{fc} is compensated by $s\Delta B$. As a result, B_{eff} is decreased so that the power-handling capability increases. The maximum power-handling capability is reached upon total field compensation at the edge of the superconductor $B_{eff}=0$.

Only for larger field changes ($|\Delta B| > 20\ \mu T$) could irreversible behavior be observed, indicating the onset of penetration and pinning of vortices inside the superconductor. Vortices for $\Delta B > 20\ \mu T$ and antivortices (opposing the B_{fc} field direction) for $\Delta B < -20\ \mu T$ nucleate in the superconductor, contributing to the asymmetry of P_{max} as a function of ΔB. The small side peaks observed left and right of the maximum in the inset of Fig. 2 can be explained by a relaxation of the magnetization upon vortex and antivortex penetration, respectively.

We can state that the power-handling capability in dc magnetic fields is strongly affected by (i) the magnetization of the superconductor, (ii) the vortex penetration and pinning, and (iii) the vortex density distribution. In the following, this behavior will be analyzed and discussed in detail and the impact of magnetization, penetrated vortices, thermal effects, and quasiparticle scattering will be investigated and discussed.

A. Impact of magnetic fields

In the discussion of Fig. 2, we interpret the impact of dc magnetic fields on the power-handling capability of YBCO coplanar resonators. In general, small magnetic fields cause a magnetization of a superconductor. This gives rise to demagnetizing effects which can alter the value of the surface magnetic field. If the surface magnetic field exceeds the penetration field, vortices start to penetrate into type-II superconductors.

In the following, we will demonstrate the impact of magnetic fields on the microwave properties by a set of experiments qualified to investigate the individual mechanisms, i.e., (i) magnetization of the superconductor, (ii) penetration of vortices, (iii) vortex pinning, and (iv) relaxation of vortex distributions.

1. Magnetization

In the Meissner state, the interior of a superconductor is field-free. An externally applied magnetic field H_0 is expelled from its interior due to screening currents which give rise to the magnetization M of the superconductor. The magnetization distorts the magnetic field outside of the superconductor. At the superconductor surface, the effective surface magnetic field H_{eff} can be calculated according to[24]

$$\mu_0 H_{eff} = \mu_0 H_0 - DM, \tag{8}$$

where D is the demagnetizing factor, which takes the geometry of the superconductor into account. Since in the Meissner state at the surface $M = -\mu_0 \cdot H_{eff}$ it follows that

$$H_{eff} = H_0/(1-D) = sH_0, \tag{9}$$

where s is a field-enhancement factor. Since $0 < D < 1$, the effective magnetic field is generally larger than the applied

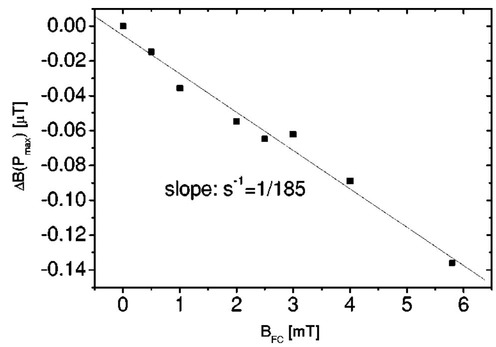

FIG. 3. Field change ΔB at P_{max} as a function of frozen-in magnetic field B_{fc}. A linear fit to the measured data gives a slope of $s^{-1}=185^{-1}$.

field. For thin superconducting films with an external magnetic field perpendicular to the surface as in our experiments, D is generally close to 1, what results in large field-enhancement factors $s \gg 1$.

For the center conductor of our coplanar resonator geometry, the field-enhancement factor can be approximated using an elliptic approximation for the superconductor cross-section giving a value of $s \approx 280$ for our geometry.[25] However, since the field enhancement is determined by the curvature of the cross section at the sides of the superconductor and since this curvature is overestimated by an elliptic approximation of a rectangular cross section, a somewhat lower value for the field enhancement than 280 can be expected.[26]

We note here that such demagnetizing effects only affect field changes in the superconducting state. Since a frozen-in magnetic field B_{fc} penetrates the superconductor in the form of a homogeneous vortex lattice, no magnetization results from B_{fc} and, thus, no demagnetizing effects are expected. The value of the surface magnetic field therefore does not differ from B_{fc}. However, demagnetizing effects do occur for a subsequent field change ΔB. Assuming that the frozen-in vortices remain pinned during the field change, the effective surface magnetic field B_{eff} can be approximated by

$$B_{eff} = B_{fc} + s\Delta B. \tag{10}$$

Based on these considerations, the fcs experiments allow the experimental determination of the demagnetizing factor. In Fig. 2 the maximum power-handling capability is given for total field compensation, i.e., $B_{eff}=0$. According to Eq. (5), in this case

$$B_{fc} = -s\Delta B. \tag{11}$$

Figure 3 shows a plot of $\Delta B(P=P_{max})$ as a function of B_{fc} for a series of experiments with different frozen-in magnetic fields. The data can be nicely fitted to linear behavior which goes through 0 and gives a field enhancement of $s=185$ corresponding to a demagnetizing factor of $D=0.9946$. This result is in excellent agreement with the theoretical expectations. For comparison, the expected demagnetizing factor for the outer electrodes is $D=0.999\,76$ ($s=4208$) which is clearly not observed. Therefore this result also proves that the power-handling capability is determined by the center conductor.

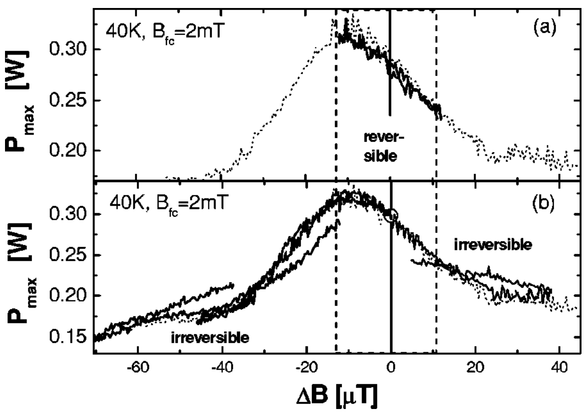

FIG. 4. Magnetic-field cycles with different amplitudes in fcs experiments reveal the underlying mechanisms of magnetization [reversible behavior in (a)] and vortex or antivortex penetration [irreversible behavior in (b)]. The gray line represents the single scan starting at $B_{fc}=2$ mT (see inset of Fig. 2).

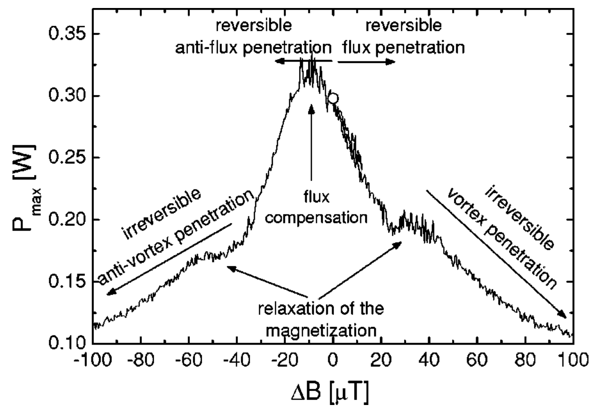

FIG. 5. Schematical fcs experiments: For small ΔB the superconductor is magnetized and the associated screening currents decrease ($\Delta B > 0$) or increase ($\Delta B < 0$) the power-handling capability reversibly. The maximum of P_{max} as a function of ΔB is characterized by total compensation of the frozen-in magnetic field. At field changes ΔB larger than a certain penetration field, vortices start to penetrate and nucleate in the superconductor accompanied by a small ancillary peaks the P_{max}. Increasing the field further, more vortices penetrate the superconductor, resulting in a monotonical decrease of P_{max} as a function of field change ΔB.

2. Vortex penetration and pinning

For infinitely extended type-II superconductors the lower critical magnetic field H_{c1} marks the transition from the Meissner phase to the mixed state, i.e., the penetration field above which vortices penetrate into the superconductor. For an infinitely extended superconducting surface, screening currents at the superconducting surface give rise to the Bean–Livingston barrier. For real devices, the penetration field depends on the geometry of the superconductor and it can be significantly lower than H_{c1}. Furthermore, the penetration barrier can be lowered or removed by Lorentz's forces due to inhomogeneous transport current densities, which might be especially efficient in stripline structures due to their peaked nature at the superconductor surface.

For a rectangular cross section of the superconductor, like the center conductor of the coplanar structure, the penetration fields have been calculated by Zeldov *et al.*[27] According to their calculation, vortices are energetically stable inside the superconductor and can therefore tunnel through a surface barrier into the superconductor for applied fields $H_0 > H_t$ with

$$H_t = H_{c1} t/2w, \tag{12}$$

while the surface barrier vanishes and collective penetration can occur for $H_0 > H_p$ with

$$H_p = H_{c1}(t/w)^{0.5}. \tag{13}$$

For the center conductor of our geometry, the values for H_t and H_p are $0.003H_{c1}$ and $0.055H_{c1}$, i.e., vortex penetration can already occur at values $H_0 \ll H_{c1}$. In this calculation, demagnetizing effects as discussed above are already taken into account.[26]

Experimentally, the underlying mechanism can be identified by cycling the external magnetic field since a magnetization gives a reversible behavior while the pinning of penetrated vortices inside the superconductor gives rise to irreversible behavior. In the fcs experiments shown in Fig. 4(a) the magnetic field of $B_{fc}=2$ mT has been frozen in. After the measurement temperature $T=40$ K was stabilized, the applied magnetic field was changed for ΔB, cycling it up to (a) small and (b) larger amplitudes ΔB_{max}, and the power-handling capability was measured [solid lines in Figs. 4(a) and 4(b), respectively]. In each plot, the noncycled behavior is plotted as an underlying dotted line.

For small amplitudes in Fig. 4(a), the power-handling capability shows a reversible behavior which can be explained by a reversible magnetization of the superconductor. Only for larger amplitudes $|\Delta B_{max}| > 20$ μT irreversible behavior, resulting from penetration and pinning of vortices inside the superconductor, is observed. Considering typical values for[28]

$$B_{c1} = 30 \text{ mT}(1 - T/T_c), \tag{14}$$

Equations (7) and (8) give for the penetration fields $B_t = 25$ μT and $B_p = 900$ μT for the sample from Fig. 4 at 40 K. Thus, the experimentally observed penetration field is considerably lower than B_p and is in very good agreement with the theoretical prediction for the tunneling barrier B_t. We note here that the tunneling of vortices into the superconductor might be efficiently facilitated by the rf current density, which might reduce the penetration barrier on both sides of the superconductor due to its oscillating nature. Vortices for $\Delta B > 0$ and antivortices (opposing the B_{fc} field direction) for $\Delta B < 0$ nucleate in the superconductor contributing to the asymmetry of P_{max} as a function of ΔB. The penetration of vortices and antivortices results in a slight relaxation of the effective magnetic field at the superconductor surface. Thus, it is accompanied with small ancillary peaks (or relaxations) of the power-handling capability (see Fig. 5).

The impact of magnetization and vortex penetration on the power-handling capability is summarized schematically in Fig. 5. We conclude that the power-handling capability in magnetic fields is governed by (i) a magnetization of the superconductor at low external fields and (ii) vortex penetration and pinning at larger external magnetic fields.

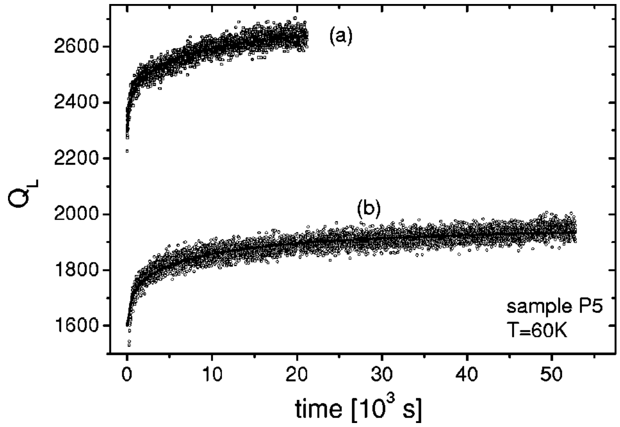

FIG. 6. Relaxation of the loaded quality factor as a function of time: (a) In the field-cooled state at 2.6 mT and $t=0$ s, Q_L is ≈ 2220. Upon suddenly switching the magnetic field off Q_L relaxes to larger values. (b) In the zero-field-cooled state at $t=0$ s, $Q_L \approx 8250$ (not shown due to scale). Upon suddenly switching the magnetic field of 2.6 mT on, Q_L is suddenly decreased to values of ≈ 1600, i.e., to lower values than in the field-cooled state, and subsequently also relaxes to larger values.

3. Vortex relaxation

At zero temperature, an inhomogeneous vortex distribution in the superconductor is sustained due to pinning. However, at nonzero temperatures, inhomogeneous vortex distributions will relax as functions of time due to thermally activated flux motion. Since the rf properties depend on the vortex distribution in the coplanar resonator as we have demonstrated above, vortex relaxation effects can be investigated by rf measurements.

Figure 6 shows typical relaxation measurements of the loaded quality factor Q_L of a coplanar resonator as a function of time. In experiment (a) the sample was field cooled in a magnetic field of 2.6 mT, and after reaching the measurement temperature of 60 K the magnetic field was suddenly switched off. In experiment (b) the sample was zero field cooled to 60 K, and at $t=0$ s a magnetic field of 2.6 mT was suddenly switched on. In both cases, a rising resonator Q value as a function of time is observed with the same relaxation parameters. The fact that in both cases a relaxation to larger Q values occurs can be explained considering the peaked rf current-density distribution and the effective surface magnetic field B_{eff} according to Eq. (5). Since the region of the peaked rf current density at the edges of the center conductor determines the resonator Q value, clearly the vortex density and screening currents at this position govern the time dependence of Q_L in these relaxation experiments.

In experiment (a) a homogeneous distribution of vortices according to an average field of 2.6 mT is frozen in. Upon switching the magnetic field off a field gradient at the superconductor surface is established, caused by pinning which can be approximated by a Bean profile.[29] This is accompanied by a sudden increase of the quality factor compared to the frozen-in state as observed in the experiment. The position of the field gradient coincides with the maximum of the microwave current distribution (see Fig. 1). The field gradient in the Bean profile can then relax due to thermally activated flux motion out of the superconductor, reducing the magnetic field in the maximum of the microwave current distribution and thereby resulting in an increase of the quality factor as a function of time as observed in Fig. 6.

In experiment (b) upon switching the magnetic field on, suddenly a large vortex density at the surface of the superconductor is introduced, reducing the Q value from its zero-field-cooled value of ≈ 8250 to values of ≈ 1600. The fact that Q_L is reduced to values lower than those observed for the field-cooled state is clearly a consequence of the larger vortex density at the edge of the superconductor, where the rf current distribution has its maximum. This inhomogeneous vortex distribution can again be approximated by a Bean profile which in this case relaxes by vortex motion into the superconductor. For this experiment the demagnetizing factor (see above) has to be taken into account, so that (i) the maximum vortex density at the edge of the superconductor will be larger than the average vortex density associated with the applied dc magnetic field and (ii) a relaxation of the Bean profile into the superconductor will reduce demagnetizing effects. This, in turn, leads to a decrease of the vortex density and screening currents at the superconductor surface. As a consequence, the resonator Q value rises as a function of time in this case, too (Fig. 6).

The time dependency of both relaxation experiments can be fitted to the Kohlrauschbehavior (line in Fig. 6)

$$Q_L = Q_1 - Q_2 e^{-(t/\tau)^\beta}, \tag{15}$$

with the same parameters $\tau \approx 5764$ s and $\beta \approx 0.45$. These values are in good agreement with values found for thermally activated vortex motion using torsion magnetometry[30]

In conclusion of this paragraph, we have confirmed that vortex relaxation is visible in microwave experiments. The characteristics of the relaxation experiments confirm our interpretation of the interaction mechanism between external dc magnetic fields and the rf properties via associated dc screening and rf transport current densities. The experimental data indicate that relaxation effects have to be taken into account for sweep rates of the applied magnetic field $dB/dt > 2.6\ \text{mT}/\tau \approx 450$ nT/s. This has been taken into account in our zfc and fcs experiments. Magnetic-field sweep rates of typically 1 nT/s have been applied; i.e., our sweep measurements are quasistatic measurements.

B. Thermal effects

At microwave frequencies, losses in superconductors occur even at arbitrary low microwave powers due to quasiparticle scattering as described by the linear surface resistance R_s, e.g., in the two-fluid model. These losses result in dissipation, and a temperature rises in the rf current carrying superconducting material. The impact of such thermal effects are determined by (i) the value of the dissipated microwave power and (ii) the thermal layout of the device. Thus, thermal effects represent a secondary device-dependent mechanism for possible nonlinear behavior in contrast to fundamental nonlinear mechanisms.

The dissipated power P_{diss} in a microwave resonator with the unloaded quality factor Q_0 and oscillating power P_{osc} is given by

$$P_{\text{diss}} = P_{\text{osc}} Q_0^{-1}. \tag{16}$$

TABLE I. Geometrical and thermal properties of the coplanar resonator materials at 77 K (see Refs. 31 and 32). λ is the specific heat conductivity in c axis direction, t is the thickness, and R_{th} is the one-dimensional (1D) thermal resistance of the layer/substrate.

	YBCO	CeO_2	Sapphire
λ [W/mK]	≈ 2	≈ 100	≈ 900
t [m]	300×10^{-9}	100×10^{-9}	0.5×10^{-3}
R_{th} [mK/W]	34.5	0.23	126.6

Therefore, this behavior is especially important in devices which have large oscillating microwave powers, i.e., which have a large power-handling capability. One specific property of coplanar devices is their low power-handling capability due to the strongly peaked current distribution. Accordingly, thermal effects are very small. However, for the investigation of possible physical nonlinear mechanisms, thermal effects have to be considered.

The coplanar resonator measured in this paper consists of a YBCO thin film deposited onto a CeO_2 buffered sapphire substrate. During measurement, the sapphire substrate is mounted to a copper shielding which serves as heat reservoir. The dissipated power heats the YBCO film and establishes a temperature gradient $\nabla T(r)$ in the device. Since no measurement showed a time evolution on a scale of the order of the duration of the measurement, it is justified to assume stationary behavior with a constant temperature gradient.

The geometrical and thermal properties are given in Table I. As an approximation, we assume one-dimensional heat transfer from the YBCO film through the substrate to the heat reservoir, which can be described by the thermal resistance

$$R_{\mathrm{th}} = t/(a\lambda), \tag{17}$$

where a is the area covered by the YBCO central conductor of the coplanar structure of 100-μm width and $\approx$44-mm length. In the stationary case, the conducted thermal energy P_{th} is then

$$P_{\mathrm{diss}} = P_{\mathrm{th}} = \Delta T/R_{\mathrm{th}}, \tag{18}$$

where ΔT is the temperature rise of the dissipating YBCO film above the temperature of the heat reservoir and $R_{\mathrm{th}} = \Sigma R_{\mathrm{th},i}$ is the total thermal resistance; the values for $R_{\mathrm{th},i}$ for the individual layers are given in Table I. Thus, clearly, the total thermal resistance of $R_{\mathrm{th}} \approx 161$ mK/W is dominated by the YBCO layer and the sapphire substrate. The heat resistance for epitaxial interfaces is typically of the order $k_{\mathrm{epi}} < 1$ mK/W for our geometry and can therefore be neglected.[33]

Using typical values for the case of the power-handling capability of $P_{\mathrm{osc}} \leqslant 1$ W and $Q_0(P_{\mathrm{osc}}) \geqslant 5000$ gives a maximum value for the dissipated power of $P_{\mathrm{diss}} \leqslant 0.2$ mW. According to Eq. (11), this gives a temperature rise for the YBCO film of $\Delta T \leqslant 32\ \mu$K above the temperature of the heat reservoir. This temperature difference is negligible in microwave experiments. The values taken in the calculation represent maximum values and the heat conductance is assumed one dimensional. However, since the width of the center conductor is only 100 μm, the cooling is quasi-two-dimensional and therefore considerably more efficient than assumed. Therefore, the presented evaluation of thermal effects represents an upper limit of the temperature effects in the YBCO layer.

We conclude that thermal effects do not play a role in any measurement presented in this paper. We note that this is a direct consequence of the strongly peaked microwave current density and the resulting low absolute power-handling capability of coplanar structures. Thus, these properties make coplanar structures ideal in investigating nonlinear effects in the absence of thermal effects.

C. Quasiparticle scattering

At rf frequencies, microwave losses of superconductors can be described by the two fluid models, which give the surface impedance

$$Z_s = R_s + iX_S \quad \text{with } R_s = \tfrac{1}{2}\mu_0^2\omega^2\sigma_n\lambda^3 \text{ and } X_s = \mu_0\omega\lambda, \tag{19}$$

where ω is the rf frequency, σ_n is the conductivity of the quasiparticles, and λ is the penetration depth. In the linear case, σ_n and λ are constant. However, a nonlinear behavior may arise when σ_n and/or λ depend/s on microwave power. Since both σ_n and λ depend on the quasiparticle density n_{QP}, any modification of it might result in a nonlinear behavior. Thus, nonlinear behavior might be caused, e.g., by rf current densities of the order of the pair-breaking critical current density $J_{c,\mathrm{PB}}$ (Ref. 34) or by magnetic fields via an increase of the average quasiparticle density due to normal vortex cores.

As we will see below in the modeling of the presented experiments and as confirmed by other authors (e.g., Willemsen *et al.*[12]), in measurements of the rf power-handling capability, the rf current density in thin-film superconducting microwave devices does not reach values of the pair-breaking critical current density. Thus, a pair-breaking-induced nonlinearity of the quasiparticle density does not seem to play a role for the observed nonlinear effects.

In order to evaluate the effect of the normal vortex cores associated with applied magnetic fields in our experiments, we consider the amount of quasiparticles which a magnetic field B introduces additionally to the intrinsic quasiparticle density $n_{\mathrm{QP}}(t)$, where t is the reduced temperature. Every normal vortex core with diameter 2ξ contains $\pi\xi^2 n_0$ quasiparticles per unit length, where n_0 is the total quasiparticle density in the normal state. A quadratic vortex lattice, for simplicity, contains one vortex per elementary cell of size $a_0 = (\phi/B)^{0.5}$ so that the average density of quasiparticles additionally introduced by the magnetic field is

$$n_B \approx \pi\xi^2(n_0 - n_{\mathrm{QP}})/a_0^2. \tag{20}$$

This value has to be compared to the intrinsic quasiparticle density $n_{\mathrm{QP}}(t)$. Using

$$n_{\mathrm{QP}}(t) = n_0 t, \quad \xi(t) = \xi_0(1-t)^{-\alpha}. \tag{21}$$

With $\gamma = 2$ and $\alpha = 0.5$ (Refs. 35 and 36), we can estimate the ratio of the quasiparticle density additionally introduced by the magnetic field to the intrinsic quasiparticle density to

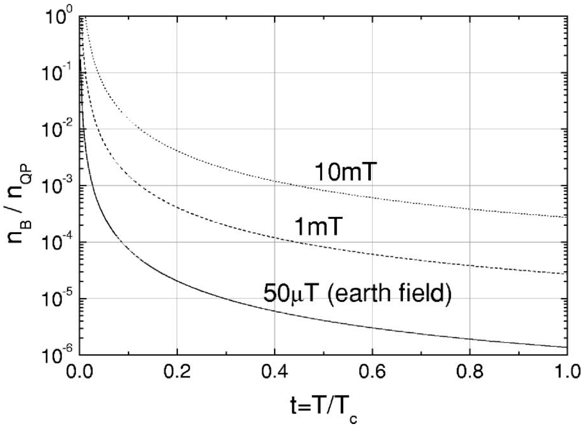

FIG. 7. Ratio of the average quasiparticle density introduced by the magnetic field to the intrinsic quasiparticle density as a function of reduced temperature for three values of the magnetic field.

$$\frac{n_F}{n_{\mathrm{QP}}} \approx \frac{\pi B \xi_0^2}{\Phi_0}\left(1-\frac{T}{T_c}\right)^{-2\alpha}\left(\left(\frac{T}{T_c}\right)^{-\gamma}-1\right). \tag{22}$$

In Fig. 7, the ratio n_B/n_{QP} is plotted as a function of reduced temperature for typical magnetic field values used in our experiments. Here, we assumed a rather large value of $\xi_0 \approx 300$ nm in order to give an upper limit of the effect. For the values of magnetic field and temperature used in our experiments the average quasiparticle density introduced by the magnetic field is less than $\approx 10^{-3}$ of the intrinsic quasiparticle density and therefore should not have a significant impact on the microwave properties. Therefore, we conclude that the increase of the average quasiparticle density caused by the normal vortex cores associated with applied magnetic fields is unlikely to be responsible for the significant decrease of the power-handling capability observed in the experiments (see Fig. 2).

IV. MODELING OF THE RESULTS

After consideration and discussion of various possible origins for the nonlinear behavior, we will finally analyze the experiments in a model that is motivated by the result that externally applied magnetic fields seem to affect the microwave properties via a current-mediated interaction. Therefore, the model considers (i) a superposition of all dc and rf current densities present in the superconductor and (ii) a limitation of the total current density.

Ambient magnetic fields lead to screening currents in the superconductor. The resulting screening current densities (j_M due to a magnetization and j_V due to vortices) superimpose the rf current density j_{rf}, yielding a total current density

$$j_{\mathrm{tot}}(\mathbf{r},t,B) = j_{\mathrm{rf}}(\mathbf{r},t,B) + j_M(\mathbf{r},B) + j_v(\mathbf{r},B) \tag{23}$$

in the coplanar resonator, where B denotes the dc magnetic field applied, e.g., in a fc, zfc, or fcs approach, and r and t indicate spatial and time dependencies. The nonlinearity implies that the total current density is limited by a maximum value $j_{\max}$ and the linear behavior is restricted to the regime $j_{\mathrm{tot}} < j_{\max}$.

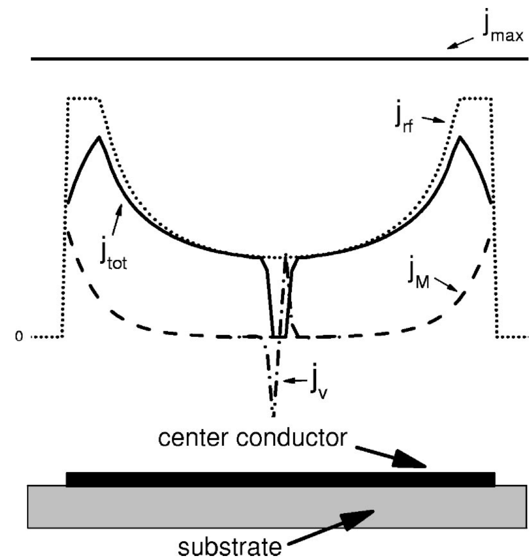

FIG. 8. Schematic of the current density distribution as a function of position on the resonator center conductor width. The zero-field current density j_{rf} (dotted line) is effectively reduced by screening current densities due to magnetization j_m (dashed line) and vortices j_v (dash-dotted line) to smaller values j_{tot} (solid line) representing a decrease of the power-handling capability in applied magnetic fields.

This model is depicted schematically in Fig. 8. Assuming that screening current densities effectively reduce the maximum transportable rf current from the zero-field value, we can approximate

$$j_{\max}(B,x) = j_{\max,B=0}(x) - j_M(B,x) - j_V(B,x). \tag{24}$$

Thus, this model automatically yields a power-handling capability that strongly depends on magnetic field. In the following, we will analyze the fc, zfc, and fcs experiments in terms of this model.

A. Field-cooled experiments: Impact of vortices

In fc experiments a homogeneous distribution of vortices in the superconductor can be assumed and magnetization effects can be neglected for not too small fields, i.e.,

$$j_{\mathrm{tot}} \approx j_{\mathrm{rf}} + j_v. \tag{25}$$

Assuming an ideal vortex lattice, the positions of the vortices in the central conductor of the resonator is given in coordinates of Fig. 1 by

$$|x_n| = [w - (2\gamma n + 1)a_0]/2, \tag{26}$$

with $n=0,1,2\ldots$, $a_0 = (\phi_o/\gamma B)^{1/2}$, and $\gamma=1$ or 0.866 for a quadratic or hexagonal vortex lattices, respectively. Since the screening current of individual vortices drops exponentially on the scale of λ, we assume that the total current density in the region $x_n \pm \alpha\lambda$ of the cross section is given by the contribution of the vortex screening current where α is of order unity. The best results are obtained for $\alpha = 1.55$. Thus, the maximum total current $I_{\mathrm{tot,max}}$ can be calculated from the experimentally determined maximum rf current $I_{\mathrm{rf,max}}(B)$ and a summation of the individual screening currents of the vortices at positions x_n within the cross section of the center conductor

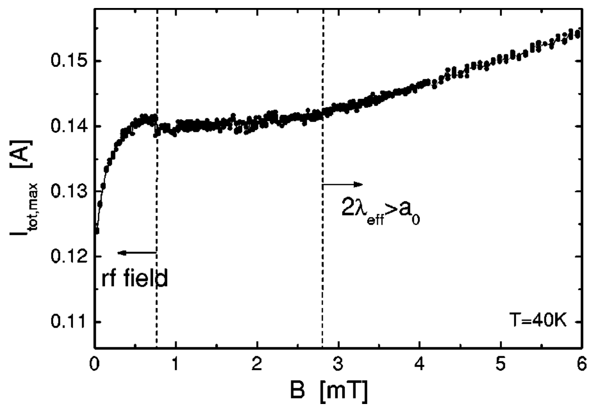

FIG. 9. Field dependence of the calculated total current [Eq. (20)] in fc experiments. The values for the rf self-field and the onset of overlap and compensation of vortex screening currents are marked and restrict the validity of Eq. (20) and, thus, the regime of constant total current.

$$I_{\text{tot,max}} = I_{\text{rf,max}} + \sum_{\text{Vortices}n} j_z(x_n) 2\lambda_{\text{eff}}\alpha. \tag{27}$$

The maximum rf current can be derived from the measurement of the power-handling capability $P_{\max}(B)$ according to

$$I_{\text{rf,max}} = \sqrt{\frac{2P_{\max}}{Z_L}}, \tag{28}$$

with the transmission line impedance $Z_L = 50\ \Omega$. Using Eq. (1) yields the maximum total current which should then be constant,

$$I_{\text{tot,max}} = I_{\text{rf,max}} \left(1 + \frac{2\lambda_{\text{eff}}\alpha}{wK\left(\frac{w}{a}\right)} \sum_{\text{Vortices}n} \left\{ \left[1 - \left(\frac{2x_n}{w}\right)^2 \right] \times \left[1 - \left(\frac{2x_n}{a}\right)^2 \right] \right\}^{-1/2} \right). \tag{29}$$

Figure 9 shows the field dependence of the maximum total current for a set of fc experiments on a typical resonator. The appropriate treatment of the impact of vortices on the power-handling capability is demonstrated by the field independence of $I_{\text{tot,max}}$ in the range of 0.5–3 mT. Deviations occur at large and at small values for the frozen-in magnetic field. At large magnetic fields $B_{\text{fc}} > 3$ mT, $a_0 < 2\lambda_{\text{eff}}$ so that the frozen-in vortices start to overlap. In this case, $I_{\text{tot,max}}$ is overestimated by Eq. (20), as can be seen in Fig. 9. The deviation from the field independence at small values for the frozen-in magnetic field $B < 0.5$ mT can be explained by the rf field itself, which can be approximated using Ampère's law

$$B_{\text{rf}} \approx \frac{\mu_0 I_{\text{rf}}}{2w}. \tag{30}$$

Using the experimental value $I_{\text{rf,max}} \approx 0.14$ A, the rf field calculates to $B_{\text{rf}} \approx 0.88$ mT, which is of the order of the field up to which the deviation from $I_{\text{tot,max}} = \text{constant}$ is experimentally observed in the small field regime.

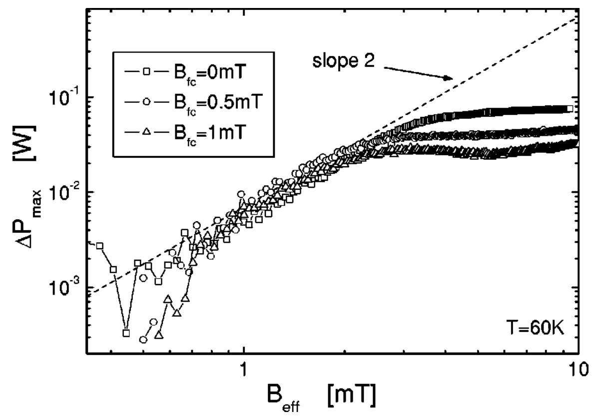

FIG. 10. Decrease of the power-handling capability $\Delta P_{\max}$ as a function of effective magnetic field B_{eff} for field-sweep experiments (zfc and fcs) for different values of the frozen-in magnetic field B_{fc}. The slope of 2 indicates good agreement with our model up to magnetic-field values for which vortex penetration occurs.

B. Field-sweep experiments: Impact of the magnetization

In contrast to fc experiments, in zfc and fcs experiments the superconductor is magnetized and only for field changes larger than some penetration field, vortices penetrate the superconductor introducing gradients in the vortex density. However, restricting our consideration to small field changes, penetration of vortices additional to those that are frozen in during cooling in the field B_{fc} can be neglected. The impact of the frozen-in vortices is then approximately constant and the change in the total current density is determined by the contributions of the rf transport and the magnetization screening current densities

$$\Delta j_{\text{tot}} \approx \Delta j_{\text{rf}} + \Delta j_M = 0. \tag{31}$$

Let us consider the case of zfc and fcs experiments for increasing field. The effective field [Eq. (5)] drops exponentially at the superconductor surface, i.e.,

$$B(x') = B_{\text{eff}} e^{-x'/\lambda} \quad \text{with } x' = |x \pm w/2|. \tag{32}$$

The resulting screening current density is given approximately by

$$j_M(x') = \frac{B_{\text{eff}}}{\lambda \mu_0} e^{-x'/\lambda}. \tag{33}$$

The total screening current can be approximated in analogy to the description of the skin effect by

$$j_M(0)\lambda t \propto B_{\text{eff}}, \tag{34}$$

where t represents the film thickness. Thus, the change of the power-handling capability can be approximated by

$$\Delta P_{\max} = P_{\max}(B_{\text{eff}}) - P_{\max}(B_{\text{fc}}) \propto (j_M(0)\lambda_{\text{eff}} t)^2 \propto B_{\text{eff}}^2. \tag{35}$$

Figure 10 shows a double logarithmic plot of $\Delta P_{\max}$ as a function of effective magnetic field B_{eff} for a typical set of zfc and fcs experiments demonstrating the excellent agreement of the data with the prediction in Eq. (26). $\Delta P_{\max}$ increases quadratically with $B_{\rm eff}$ and, even more, all data (zfc and fcs for different fields $B_{\rm fc}$) fall in one line.

A deviation from the quadratic dependence is observed at higher fields starting at $B_{\rm eff} \approx 2-4$ mT or, in terms of field change, at $\Delta B \approx 10-20\ \mu$T. We ascribe this deviation to the geometrical barrier against vortex penetration[27] which corresponds to the Bean–Livingston barrier for the special case of a rectangular superconductor cross section. Using Eqs. (7) and (8), vortices are expected to be energetically stable for magnetic fields larger than $B_t \approx 15\ \mu$T, whereas the surface barrier is expected to vanish for magnetic fields larger than $B_p \approx 500\ \mu$T for the sample shown in Fig. 10 at 60 K. Since demagnetizing effects are included in Zeldov's calculation, the field change ΔB has to be compared to the barrier directly. The experimental value is considerably lower than B_p and in excellent agreement with the theoretically predicted value for B_t. Therefore, we conclude that we observe vortex penetration into the superconductor as soon as they are energetically stable inside the superconductor. The surface barrier, which is still present at magnetic fields $B_t < B < B_p$, might be overcome, e.g., due to the microwave current density, which imposes large Lorentz's forces on vortices especially in the surface region. Penetrated vortices lead to an additional contribution to the total current in the superconductor, and, thus, the increase of $\Delta P_{\rm max}$ as a function of effective magnetic field $B_{\rm eff}$ is reduced from the quadratic law for larger $B_{\rm eff}$.

C. Zero-field experiments

Finally, zero-field measurements are discussed in terms of our model. Generally, the rf current density profile shows a maximum at the edges of the superconducting resonator. According to Eq. (1) the maximum of the current density is given by

$$j_{\rm rf,max} = \frac{\sqrt{2P_{\rm max}}}{K(w/a)}[Z\lambda_{\rm eff}wt^2(1-(w/a)^2)]^{-1/2}. \qquad (36)$$

Thus, the maximum current density in the superconductor can be derived from experimental values of $P_{\rm max}$. Figure 11 shows the resulting temperature dependence of $j_{\rm rf,max}$ for a typical resonator patterned from epitaxial YBCO films. For comparison, we also show typical linear temperature dependencies of the dc critical current density with values $j_c(77\ {\rm K})$ between 1 and 3 MA/cm^2 (Ref. 37) and the pair breaking critical current density as predicted from the Ginzburg–Landau theory according to[24]

$$j_{c,\rm PB} = \frac{8\sqrt{2}B_c(0)}{3\sqrt{3}\lambda_L(0)}\left(1-\frac{T}{T_c}\right)^{1,5}. \qquad (37)$$

Two interesting aspects should be noticed: (i) the experimental values derived from our experiments for $j_{\rm rf,max}$ increase linearly with temperature and (ii) the order of magnitude is $j_{\rm rf,max}(77\ {\rm K}) \approx 10^{10}$ Am^{-2} and $j_{\rm rf,max}(10\ {\rm K}) \approx 10^{11}$ Am^{-2}. Both the temperature dependence and the magnitude of the maximum rf current density are in excellent agreement with the dc critical current for typical YBCO thin films. This suggests that the limiting current density for the onset of nonlinear microwave behavior is given by the dc critical current of the superconductor. A relation between microwave-power-handling and pair-breaking mechanisms could not be verified by our experiments.

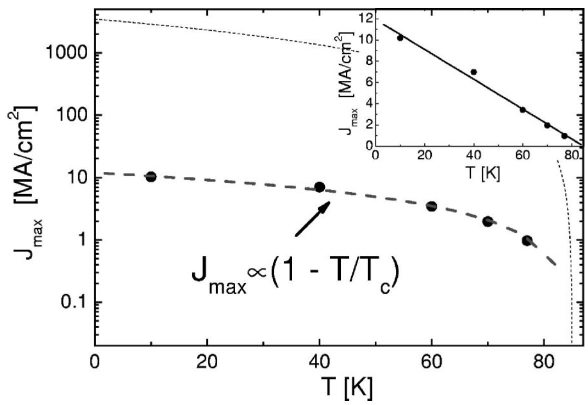

FIG. 11. Comparison of the temperature dependence of the maximum rf current density for a coplanar YBCO resonator (solid dots) with typical values for the dc critical current density expected for the depinning mechanism j_c (dashed lines) and pair-braking critical current density $j_{c,\rm PB}$ (dotted line). The solid lines in the graph and inset are linear fits to the experimental data. The inset demonstrates the linear behavior of the experimental values which is in agreement with the temperature dependence of j_c.

V. SUMMARY AND CONCLUSIONS

We have presented a concise investigation of the power-handling capability of coplanar resonators made from epitaxial YBCO thin films in small magnetic fields, employing field-cooled, zero-field-cooled and field-sweep techniques. We have shown that coplanar devices are especially useful in the investigation of the fundamental mechanism that limits the power-handling capability of high-temperature superconducting (HTS) devices. Their low absolute power-handling capability allows to neglect thermal effects. By using epitaxial thin films, which do not contain large-angle grain boundaries, grain-boundary Josephson junctions should have no impact on the microwave properties. Since coplanar devices exhibit a characteristic current distribution which is peaked at the edges of the coplanar center conductor, they allow a local investigation of the power-handling capability via a careful analysis of introduced magnetization and vortex distributions.

We have found and demonstrated by field-cycling experiments that magnetic fields affect the microwave properties via (i) a magnetization of the superconductor and (ii) penetrated vortices. Both mechanisms result in a characteristic decrease of the power-handling capability of the coplanar resonator as a function of the applied magnetic field.

All experiments in static and swept magnetic fields as well as in zero magnetic field could be consistently understood and described in terms of a simple model for the power-handling capability based on a superposition of all current densities in the resonator and a limitation of the total current density. The model is motivated by the experimental observation that the power-handling capability in small magnetic fields is governed by the surface value of the magnetic field or vortex density, since here screening currents coincide with the maximum of the peaked rf transport current density.

Both demagnetizing effects and penetration barriers against the penetration of vortices are observed in the experiments, and experimental values are in good agreement with theoretical expectations.

Relaxations of inhomogeneous vortex distributions affect the microwave properties. Our relaxation experiments could be described by a Kohlrausch behavior, with parameters in agreement with literature values for thermal vortex relaxation. Since these relaxation time scales are about two orders of magnitude longer than what is typical for the determination of the power-handling capability, the vortex relaxation does not affect our investigations of the power-handling capability. Furthermore, we have shown that thermal effects and changes of the quasiparticle density caused by the applied magnetic fields should not play a role in our measurements.

In conclusion, we have found strong experimental evidence that the fundamental mechanism that limits the power-handling capability in HTS in the absence of thermal and grain-boundary effects (i) is current driven and (ii) that the limiting scale for the onset of nonlinear microwave effects is given by the dc critical current density j_c associated with the depinning mechanism.

ACKNOWLEDGMENTS

We acknowledge helpful discussions with E.H. Brandt. This work has been supported by the ESF Vortex program.

[1] P. Lahl and R. Wördenweber, Appl. Phys. Lett. **79**, 512 (2001).
[2] J. C. Booth, L. R. Vale, and R. H. Ono, Physica C **357–360**, 1516 (2001).
[3] A. G. Zaitsev *et al.*, Appl. Phys. Lett. **79**, 4174 (2001).
[4] W. Hu *et al.*, Appl. Phys. Lett. **75**, 2824 (1999).
[5] J. H. Claassen *et al.*, Supercond. Sci. Technol. **12**, 714 (1999); Appl. Phys. Lett. **74**, 4023 (1999).
[6] P. P. Nguyen *et al.*, Phys. Rev. B **51**, 6686 (1995).
[7] M. A. Hein, Supercond. Sci. Technol. **10**, 867 (1997).
[8] D. E. Oates *et al.*, Physica C **372–376**, 462 (2002).
[9] Y. M. Habib *et al.*, Appl. Phys. Lett. **73**, 2200 (1998).
[10] H. Xin *et al.*, Phys. Rev. B **65**, 214533 (2002).
[11] D. Dimos, P. Chaudhari, and J. Mannhart, Phys. Rev. B **41**, 4038 (1990).
[12] B. A. Willemsen *et al.*, Phys. Rev. B **58**, 6650 (1998).
[13] T. Dahm, D. J. Scalapino, and B. A. Willemsen, J. Supercond. **12**, 339 (1999).
[14] D. E. Oates *et al.* Supercond. Sci. Technol. **17**, S290 (2004).
[15] R. Wördenweber, Supercond. Sci. Technol. **12**, R86 (1999).
[16] E. H. Roderic and E. M. Wilson, Nature (London) **194**, 1167 (1962).
[17] R. E. Glover and H. T. Coffey, Rev. Mod. Phys. **36**, 299 (1964).
[18] T. Van Duzer and C. W. Turner *Principles of Superconductive Devices and Circuits* (Elsevier, New York, 1981).
[19] G. H. Owyanga and T. T. Wu, IRE Trans. Antennas Propag. **AP-6**, 49 (1958).
[20] M. Kumar and B. N. Das, J. Inst. Eng. (India), Electron. Tele-Commun. Eng. Div. **23**, 137 (1977).
[21] J. Pearl, Appl. Phys. Lett. **5**, 65 (1964).
[22] I. B. Vendik, O. G. Vendik, and D. I. Kaparkov, *Superconductor Microwave Technology, Part II: Superconducting Microwave Circuits*, edited by E. Kollberg (Chalmers University of Technology, Göteborg, Sweden, 1996).
[23] M. Pannetier *et al.*, Phys. Rev. B **67**, 212501 (2003).
[24] M. Tinkham, *Introduction to Superconductivity* (McGraw-Hill, New York, 1996).
[25] H. W. Weber and O. Hittmair, *Supraleitung* (Verlag Karl Thiemig, München, 1979).
[26] E. H. Brandt (private communication).
[27] E. Zeldov *et al.*, Phys. Rev. Lett. **73**, 1428 (1994).
[28] R. Wördenweber in *Anwendungen/Vakuumbeschichtung, Supraleitende Schichten*, edited by G. Kienel (Springer, Berlin, 1993), Vol. 4, p. 45; T. K. Worthington *et al.*, Phys. Rev. Lett. **59**, 1160 (1987).
[29] C. P Bean, Phys. Rev. Lett. **8**, 250 (1962).
[30] C. W. Hagen, Ph.D. thesis, Vrije Universiteit Te Amsterdam, 1991; C. W. Hagen *et al.*, Physica C **153**, 322 (1988).
[31] *Physical Properties of High Temperature Superconductors*, edited by D. M. Ginsberg (World Scientific, Singapore, 1989).
[32] Y. M. Touloukian and E. H. Buyco, *Thermophysical Properties of Matter, Specific Heat, Nonmetallic Solids*, TPRC Data Series Vol. 5 (Plenum, New York, 1970).
[33] C. D. Marshall *et al.*, J. Appl. Phys. **73**, 850 (1993).
[34] T. Dahm and D. J. Scalapino, Appl. Phys. Lett. **69**, 4248 (1996).
[35] D. A. Bonn *et al.*, Phys. Rev. B **47**, 11314 (1993).
[36] S. Orbach-Werbig, Ph.D. thesis, Rheinisch Westfälische Technische Hochschule (RWTH) Aachen (2000).
[37] B. Dam *et al.*, Nature (London) **399**, 439 (1999).